BJP BRITISH JOURNAL OF PHARMACOLOGY

BPS BRITISH PHARMACOLOGICAL SOCIETY

British Journal of Pharmacology (2010), 160, 1941–1952

0007-1188/10
www.brjpharmacol.org

RESEARCH PAPER

Electrophysiological classification of P2X7 receptors in rat cultured neocortical astroglia

W Nörenberg, J Schunk, W Fischer, H Sobottka, T Riedel, JF Oliveira*, H Franke and P Illes

Rudolf-Boehm-Institute of Pharmacology and Toxicology, University of Leipzig, Leipzig, Germany

Background and purpose: P2X7 receptors are ATP-gated cation channels mediating important functions in microglial cells, such as the release of cytokines and phagocytosis. Electrophysiological evidence that these receptors also occur in CNS astroglia is rare and rather incomplete.
Experimental approach: We used whole-cell patch-clamp recordings to search for P2X7 receptors in astroglial–neuronal co-cultures prepared from the cerebral cortex of rats.
Key results: All the astroglial cells investigated responded to ATP with membrane currents, reversing around 0 mV. These currents could be also detected in isolated outside-out patch vesicles. The results of the experiments with the P2X [α,β-methylene ATP and 2′-3′-O-(4-benzoyl) ATP] and P2Y receptor agonists [adenosine 5′-O-(2-thiodiphosphate), uridine 5′-diphosphate, uridine 5′-triphosphate (UTP) and UDP-glucose] suggested the involvement of P2X receptors in this response. The potentiation of ATP responses in a low divalent cation or alkaline bath, but not by ivermectin, made it likely that a P2X7 receptor is operational. Blockade of the ATP effect by the P2X7 antagonists Brilliant Blue G, calmidazolium and oxidized ATP corroborated this assumption.
Conclusions and implications: Rat cultured cortical astroglia possesses functional P2X7 receptors. It is suggested that astrocytic P2X7 receptors respond to high local ATP concentrations during neuronal injury.
British Journal of Pharmacology (2010) **160,** 1941–1952; doi:10.1111/j.1476-5381.2010.00736.x

Keywords: astrocytes; astroglia; extracellular ATP; P2X7 receptors; glial necrosis; glial proliferation

Abbreviations: 2MeSATP, 2-(methylthio) adenosine 5′-triphosphate; α,βmeATP, α,β-methylene adenosine 5′-triphosphate; ADPβS, adenosine 5′-O-(2-thiodiphosphate); BBG, Coomassie Brilliant Blue G; BzATP, 2′-3′-O-(4-benzoyl) adenosine 5′-triphosphate; CAL, calmidazolium; CBX, carbenoxolone; DPCPX, 1,3-dipropyl-8-cyclopentylxanthine; GFAP, glial fibrillary acidic protein; IVM, ivermectin; LY, Lucifer yellow; oATP, adenosine 5′-triphosphate periodate oxidized; PPADS, pyridoxal-5′-phosphate-6-azophenyl-2′,4′-disulphonic acid; TNP-ATP, 2′-3′-O-(2,4,6-trinitrophenyl) adenosine 5′-triphosphate; UDP, uridine 5′-diphosphate; UDP-Gluc, uridine 5′-diphosphoglucose; UTP, uridine 5′-triphosphate

Introduction

Purine and pyrimidine nucleotides are intercellular messenger molecules engaged in important regulatory functions in the peripheral as well as central nervous systems. The role of ATP as a co-transmitter in fast synaptic neurone-to-neurone signalling has thus been firmly established during the last years (Burnstock, 2007). However, growing evidence indicates that its involvement in information transfer is broader than originally assumed. According to the concept of tripartite synapses, the nucleotide may also be implicated in mutual neurone–astrocyte crosstalk and may contribute to astrocyte–astrocyte communication as well (Araque *et al.*, 1999; Burnstock, 2007). Hence, astrocytes and neurones appear to be integrated by purinergic signalling in functional circuits.

Considerable interest, therefore, exists in defining the receptor subtypes involved in neurone–astrocyte crosstalk and astrocyte–astrocyte communication. The effects of extracellular ATP and related nucleotides are brought about by two groups of cell-surface P2 receptors. The first group comprises P2X receptors, ligand-gated cation channels, which are Ca^{2+} permeable, whereas the second group consists of G protein-coupled P2Y receptors, most of which can mobilize Ca^{2+} from its intracellular stores. Seven different P2X subunits have been cloned to date, which assemble into either homotrimeric (P2X1–7) or heterotrimeric receptor proteins (P2X1/2, P2X1/4, P2X1/5, P2X2/3, P2X2/6, P2X4/6 and P2X4/7; Jarvis

Correspondence: Dr Wolfgang Nörenberg, Rudolf-Boehm-Institute of Pharmacology and Toxicology, University of Leipzig, Härtelstrasse 16-18, D-04107 Leipzig, Germany. E-mail: Wolfgang.Noerenberg@medizin.uni-leipzig.de
*Present address: Life and Health Sciences Research Institute, School of Health Sciences, University of Minho, Braga, Portugal.
Received 9 December 2009; revised 3 February 2010; accepted 8 February 2010

and Khakh, 2009), whereas the group of mammalian P2Y receptors comprises eight hitherto known subtypes ($P2Y_{1–2}$, $P2Y_4$, $P2Y_6$, $P2Y_{11–14}$; von Kügelgen, 2006; receptor nomenclature follows Alexander *et al*., 2009).

P2X7 receptors have been identified at both peripheral and central immunocytes such as macrophages, lymphocytes and microglia, where they interact with several partners including cytoskeletal proteins (Sperlágh *et al*., 2006; Surprenant and North, 2009). These receptors are stimulated by high extracellular concentrations of ATP and, in consequence, initiate immune responses, for example, via the maturation and release of interleukin-1β. In addition, they are involved in both apoptosis/necrosis and proliferation of immunocompetent cells including astrocytes (Franke and Illes, 2006). The activation of P2X7 receptors at the plasmalemma of cultured astrocytes from rats and mice has been reported to initiate the entry of external Ca^{2+} and the subsequent increase of cytoplasmic Ca^{2+} (Fumagalli *et al*., 2003; Nobile *et al*., 2003). In addition, astrocytic P2X7 receptors mediate the release of glutamate (Duan *et al*., 2003), GABA (Wang *et al*., 2002) and even ATP itself (Suadicani *et al*., 2006), possibly subserving astrocyte–neurone communication or modulating the outcome of CNS injury. Although all these experiments supplied a wealth of indirect evidence for the presence of P2X7 receptors at cultured astrocytes, direct electrophysiological measurements of cationic fluxes supporting this assumption are rare and rather incomplete (Duan *et al*., 2003). Patch-clamp recordings from acutely dissociated astrocytes or from astrocytes in brain slices additionally increased the ambiguity of this issue by reporting the exclusive presence of P2X7 homomeric receptors (Fellin *et al*., 2006) and P2X1/5 heteromeric receptors (Lalo *et al*., 2008), or even the complete absence of any P2X receptor type (Jabs *et al*., 2007).

Thus, the present study was aimed to re-investigate by means of whole-cell patch-clamp recordings the functionality of astrocytic P2X receptor subtypes. To minimize the problems inevitably associated with brain slice recordings, such as diffusion barriers supporting the breakdown of ATP by ectoenzymes, as well as the desensitization of P2X receptors, by subthreshold concentrations of the nucleotide during its delayed dispersal or during its retarded washout, we chose astroglial cells contained in mixed glial–neuronal cell cultures from the cerebral cortex of rats as a reductionist model. Our data obtained with this preparation clearly indicate the functional presence of P2X7 in these astrocyte-like cells. A preliminary account of some of the results has appeared in abstract form (Fischer *et al*., 2008).

Methods

Isolation and in vitro *maintenance of rat neocortical astrocytes*

Co-cultures of rat neocortical astroglia and neurones were, with some modifications, prepared as previously described (Fischer *et al*., 2009). Pregnant Wistar rats were decapitated at gestational day 16 in deep carbon dioxide anaesthesia, and the fetal neocortical hemispheres were dissected, freed of the hippocampus, minced and pooled in ice-cold (4°C) Hank's balanced salt solution (HBSS; Invitrogen, Karlsruhe, Germany). Tissue samples were then dissociated by trypsin ($1.25\ mg{\cdot}mL^{-1}$) (Invitrogen) in HBSS for 8 min and at 37°C. Enzymatic digestion was stopped by heat-inactivated fetal calf serum (FCS; 20%) (Seromed, Berlin, Germany) added to a 1:1 mixture of Dulbecco's modified Eagle's medium and Ham's nutrient mixture F12 also containing 2.5 mM L-alanyl-L-glutamine (Invitrogen). After gentle trituration through a fire-polished Pasteur pipette and centrifugation (984× *g* for 5 min), the remaining cell pellet was taken up and resuspended in the culture medium of the above constitution, supplemented in addition with 36 mM D(+)-glucose, 15 mM HEPES (pH 7.4 with NaOH) and $50\ \mu g{\cdot}mL^{-1}$ gentamicin. The final cell suspension was then poured into poly-L-lysine-coated 35 mm diameter polystyrol culture dishes at a plating density of $\sim 5 \times 10^3\ cm^{-2}$.

Cultures were maintained in 2 mL of the culture medium at 37°C in a humidified atmosphere of 5% CO_2 in air. To prevent excessive proliferation of glial cells, 10 μM of cytosine-β-D-arabinofuranosid was added for 24 h at day 6 *in vitro*, and the FCS content in the culture medium was reduced to 10% thereafter. Cultures were then used on days 12–16 *in vitro* for all experiments.

Electrophysiology: experimental solutions

Astrocytes in primary neocortical glia–neurone co-cultures have been previously found to be extensively coupled by gap junctions (Murphy *et al*., 1993). All bath solutions, therefore, contained 100 μM of the gap junction blocker carbenoxolone (CBX; Sigma-Aldrich, Taufkirchen, Germany), which was present for at least 15 min prior to the beginning of the experiments and, in addition, throughout their time course.

The standard bath solution contained (in mM): NaCl 140, KCl 2.5, $CaCl_2$ 1.0, $MgCl_2$ 1.2, HEPES 25 and glucose 10.5 ($\sim 315\ mOsm{\cdot}L^{-1}$, pH 7.3 with NaOH). A slightly different extracellular saline, intended to test the sensitivity of ATP-induced currents against the blocking actions of extracellular Ca^{2+}, Mg^{2+} and H^+, was prepared by omitting $MgCl_2$ and lowering the $CaCl_2$ content to 0.1 mM (low divalent cation (DIC)-containing bath; Figures 3 and 4). Acidification (pH 6.3) and alkalinization (pH 8.3; Figure 4) were achieved by adding the required amounts of HCl and NaOH respectively. The pipette solution comprised (in mM): either potassium gluconate 140 (Figures 1 and 2A,B) or caesium methanesulphonate 130 (Figures 2C–4), NaCl 10, $CaCl_2$ 0.2, $MgCl_2$ 3, HEPES 10, EGTA 10, Mg-ATP 4 and Li-GTP 0.3. It had an osmolarity of $\sim 305\ mOsm{\cdot}L^{-1}$ and a pH adjusted to 7.2 with either KOH or CsOH as appropriate.

Osmolarities of all experimental salines were routinely checked by means of a freezing point semi-micro osmometer (Type ML, Knauer, Berlin, Germany). The liquid junction potentials, given as potential of the bath solution with respect to the pipette solution, were computed by JPCalc software (Barry, 1994) and amounted to 14 and 11 mV in the case of potassium gluconate and caesium methanesulphonate being used as the main ingredients of the internal solution respectively.

Electrophysiology: recording procedures

Conventional whole-cell voltage- and current-clamp-, or in some experiments, excised outside-out patch recordings were

performed at room temperature (20–24°C) by means of an extracellular patch-clamp amplifier (EPC-9, HEKA, Lambrecht, Germany) interfaced via an ITC-16 DA/AD converter (InstruTECH, Bellmore, NY, USA) to a standard laboratory computer. Pulse software (Version 8.80, HEKA) was used throughout for the control of experimental parameters and data recording.

Patch pipettes were prepared from borosilicate glass capillaries (GB150F-8P, Science Products GmbH, Hofheim, Germany) by a horizontal puller (Model P-87, Sutter Instruments, Novato, CA, USA). When filled with intracellular solution, pipette resistances were typically 2–5 MΩ.

The holding potential (–80 mV) was set, and the values for reversal potential were corrected by taking into account the respective liquid junction potential values given above. Currents in response to voltage steps were sampled at 30 kHz and low-pass filtered at 10 kHz prior to storage. Membrane currents in response to the P2X/P2Y receptor agonist ATP (and some of its structural analogues) were sampled at 3 kHz and filtered at 1 kHz.

Receptor agonists, modulators and antagonist were focally applied by means of the application cannula (100 µm inner diameter) of a solenoid valve-driven pressurized superfusion system (DAD-12, ALA Scientific Instruments Inc., Farmingdale, NY, USA), placed in the immediate vicinity (10–20 µm) of the cell under investigation. The exchange rate was estimated at the end of recordings from the rise time between 20% and 80% of the peak response to a 30% dilution of the bath solution with deionized water, applied to the open tip of the patch pipette. It was 153.7 ± 22.7 ms ($n = 25$) and, hence, was well within the times of agonist application (3–40 s).

Electrophysiology: data analysis

Membrane capacitance and series resistance were determined from capacitive transients using the Pulse software-controlled inbuilt circuitry of the EPC-9 amplifier. Data from cells in which this compensation procedure failed were not analysed further. Membrane capacitance and series resistance (partially compensated by 60–80%) were monitored repeatedly during the experiments. They did not change significantly over the course of the trials (usually ~15 to ~30 min), hence indicating stable recording conditions.

Electrophysiological data were evaluated with a combination of PulseFit and PulseTools software (Version 8.80, HEKA). SigmaPlot (Version 10.0, Systat Software Inc, San José, CA, USA) was used for curve fitting and plotting purposes.

Membrane currents were measured as peak responses with respect to the holding current level. They were normalized for differences in cell size (membrane capacitance), and current densities (pA·pF^{-1}) are reported, except for data from outside-out patches, which are given in pA. However, the currents evoked by P2 receptor agonists, in some experiments, did not fully reach their maximum (e.g. the ATP-induced current in Figure 3B). In these cases, the peak current attained within the time of agonist application was used. Sensitivity of a cell from a particular set of experiments to a given agonist was taken for granted when the effect of this agonist surmounted a threshold set by the mean ± 3 times SEM current, which was evoked by pressure application of drug-free bath solution in the same set of experiments.

Reversal potentials of ATP-induced currents were obtained from first-order polynomials fitted to the net agonist-induced currents at various command potentials (V_c; see Figure 2C). The conductance increase caused by ATP was then calculated from these net agonist-induced currents by:

$$G = \frac{I}{(V_c - E_x)} \quad (1)$$

where G is the specific conductance (pS·pF^{-1}), I is the agonist-evoked net current (pA·pF^{-1}) at a V_c of +40 mV and E is 0 mV, the assumed equilibrium potential for ion fluxes through non-selective cation channels.

The means of ATP [and 2′-3′-O-(4-benzoyl) ATP (BzATP; Sigma-Aldrich)] concentration-response data were fitted to a three-parameter logistic function (Hill equation) of the form:

$$I = \frac{I_{max}[A]^{nH}}{[A]^{nH} + EC_{50}{}^{nH}} \quad (2)$$

where I is the experimentally observed current in response to agonist concentration [A], I_{max} is the extrapolated maximum current, EC_{50} is the agonist concentration producing 50% of I_{max}, and nH is the Hill coefficient.

Immunocytochemistry

In order to evaluate both the histochemical phenotype of the recorded cells and the effectiveness of gap junction uncoupling by CBX, one presumed astrocyte per culture dish was loaded during whole-cell recordings in the standard bath for a total of 15 min, during which time the tracer was allowed to spread, with the gap junction permeable dye Lucifer yellow (LY; Sigma-Aldrich) added at 1 mg·mL^{-1} to the K-gluconate pipette solution. Cells were, to facilitate the passage of the negatively charged LY, voltage clamped to –100 mV, except for the short period (~2 min) necessary for the electrophysiological characterization [recording of current-voltage (*I-V*) curves].

Post-recording LY detection was then performed with a rabbit anti-LY antibody (Invitrogen) using carbocyanine (Cy)3-conjugated donkey anti-rabbit IgG (Jackson ImmunoResearch, West Grove, PA, USA) as a fluorophore. LY detection was combined with immunolabelling of the astrocyte marker glial fibrillary acidic protein (GFAP) by a mouse anti-GFAP antibody (Sigma-Aldrich), visualized by fluorescent Cy5-conjugated donkey anti-mouse IgG (Jackson ImmunoResearch). In addition, the nucleic acid probe Hoechst 33342 (Hoe), with autofluorescence under ultraviolet light, was used to identify astrocytic cell nuclei.

The processing of cultures for immunocytochemistry was as follows: culture dishes containing the dye-filled neocortical cells were washed in phosphate buffered saline (PBS; 0.1 M and pH 7.4) and fixed in ice-cold paraformaldehyde (4% in PBS) for 20 min, followed by intensive washing in PBS. Subsequent to rinsing with PBS, cells were pretreated for permeabilization and blocking of non-specific binding with 0.3% Triton X-100 (Carl Roth GmbH, Karlsruhe, Germany) and 5% FCS, respectively, in Tris-buffered saline (TBS; 0.05 M and pH 7.6) for 30 min. Then, the cultures were incubated with a mixture containing the primary antibodies (rabbit anti-LY,

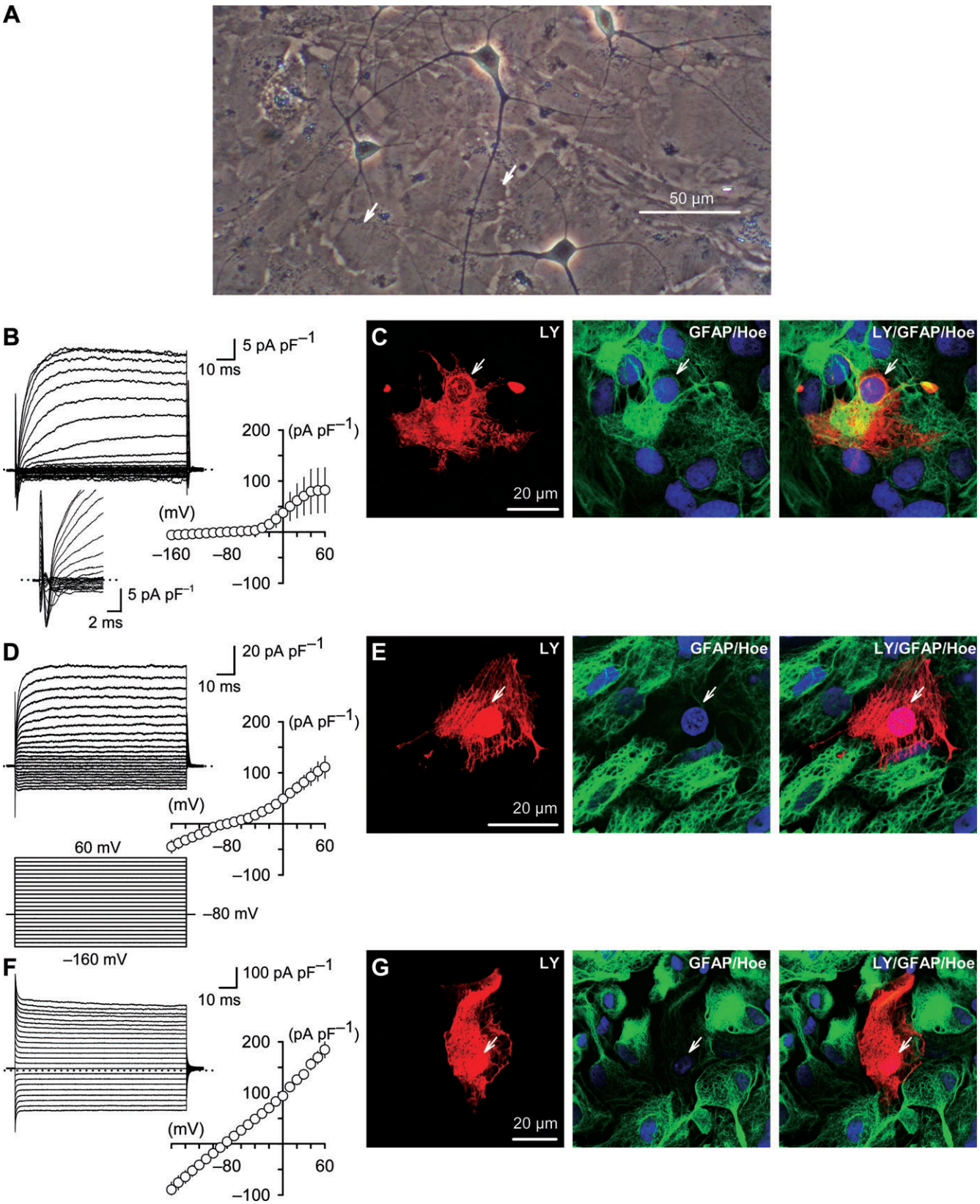
A
50 µm
B
5 pA pF−1
10 ms
200
(pA pF−1)
100
(mV)
−160
−80
60
−100
5 pA pF−1
2 ms
C
LY
20 µm
GFAP/Hoe
LY/GFAP/Hoe
D
20 pA pF−1
10 ms
200
(pA pF−1)
100
(mV)
60 mV
−80
60
−100
−80 mV
−160 mV
E
LY
20 µm
GFAP/Hoe
LY/GFAP/Hoe
F
100 pA pF−1
10 ms
200
(pA pF−1)
100
(mV)
−80
60
−100
G
LY
20 µm
GFAP/Hoe
LY/GFAP/Hoe

Figure 1 Morphological, electrophysiological and immunocytochemical phenotyping of rat cultured cortical astrocytes. (A) Microphotograph obtained under phase contrast optics of a mixed glial–neuronal co-culture from rat neocortex. Arrows indicate typical astroglial cells similar to those chosen for electrophysiological recordings. Four overlying multipolar neurones with dendrite-like processes are also visible. (B, D, F) Whole-cell voltage-clamp recordings from three different presumed astrocytes showing an outwardly rectifying (B), variably rectifying (D) or a passive (linear) membrane current profile (F) in response to the voltage-step protocol exemplified between (D) and (F) (holding potential –80 mV, standard bath, K^+-based pipette solution). Transient inward currents (inset below B) preceded the outward currents in the outwardly rectifying cell. The current-voltage (*I-V*) relationships shown were constructed from current amplitudes in the middle of the 100 ms voltage steps and were measured in three (B), five (D) and six (F) presumed astrocytes respectively. The dotted lines in the current traces indicate in this and all subsequent figures the 0 current level. (C, E, G) Confocal microscopy images from the cells in (B), (D) and (F), filled during recordings with Lucifer yellow (LY), showing (from left to right) the red carbocyanine (Cy)3 immunofluorescence for LY and the Cy5 green colour-coded immunofluorescence for the astrocyte marker glial fibrillary acidic protein (GFAP) together with the ultraviolet light excited blue fluorescence for the nucleic acid probe Hoechst 33342 (Hoe), as well as the co-localization of LY with GFAP and Hoe. Although sometimes only weak, yet detectable [e.g. in (E)], all glial cells investigated by this way ($n = 14$, $N = 6$) were positive for GFAP and, hence, were astrocyte like. As detailed in Methods, recordings were obtained with 100 μM of the gap junction blocker carbenoxolone (CBX) in the bath. Note that only one Hoe-positive nucleus (arrows) per cell was co-localized with LY, indicating that CBX had effectively suppressed syncytial communication.

1:1000, plus mouse anti-GFAP, 1:1000) together with 0.1% Triton X-100 and 5% FCS in TBS for 24 h and at 4°C. After being rinsed in TBS, the cells were exposed to the secondary antibodies (Cy3-conjugated donkey anti-rabbit IgG, 1:1000, and Cy5-conjugated donkey anti-mouse IgG, 1:100) for 2 h and at room temperature in TBS containing 0.3% Triton X-100 and 5% FCS. Hoe (17 μM) was added 10 min before the end of this incubation period. After being washed, the preparations were embedded in Immu-Mount (ThermoScientific, Pittsburgh, PA, USA) and cover slipped.

Immunofluorescence was investigated by means of an inverted confocal laser scanning microscope (510 Meta, Zeiss, Oberkochen, Germany) at excitation wavelengths of 543 nm (helium/neon1, red Cy3 immunofluorescence) and 633 nm (helium/neon2, green colour-coded Cy5 immunofluorescence), whereas an ultraviolet laser (351–362 nm) was used to evoke the blue-cyan Hoe autofluorescence. The extent of gap junction coupling in the presence of CBX was then evaluated by counting the Hoe-positive nuclei co-localized with the staining for LY and GFAP.

Materials

The following chemicals were used: AMPA, 1,3-dipropyl-8-cyclopentylxanthine (DPCPX), muscimol and tetrodotoxin (TTX) (Biotrend, Köln, Germany); Triton X-100 (Carl Roth GmbH); Dulbecco's modified Eagle's medium plus nutrient mixture F12 (1:1) plus 2.5 mM L-alanyl-L-glutamine (Dulbecco's modified Eagle's medium/F12 1:1 with GlutaMAX™ I), HBSS, Hoe, rabbit anti-LY antibody and trypsin (Invitrogen); Cy5-conjugated donkey anti-mouse IgG and Cy3-conjugated donkey anti-rabbit IgG (Jackson ImmunoResearch); FCS (Seromed); 2-(methylthio) ATP (2MeSATP), adenosine 5′-O-(2-thiodiphosphate) (ADPβS), ATP, α,β-methylene ATP (α,βmeATP), ATP periodate oxidized (oATP), BzATP, calmidazolium (CAL), CBX, Coomassie Brilliant Blue G (BBG), cytosine-β-D-arabinofuranosid, gentamicin, ivermectin (IVM), LY, mouse anti-GFAP antibody, poly-L-lysine, pyridoxal-5′-phosphate-6-azophenyl-2′,4′-disulphonic acid (PPADS), suramin, 2′-3′-O-(2,4,6-trinitrophenyl) ATP (TNP-ATP), uridine 5′-diphosphate (UDP), uridine 5′-diphosphoglucose (UDP-Gluc), uridine 5′-triphosphate (UTP) and ZnCl (Sigma-Aldrich).

Stock solutions (0.1–100 mM) of drugs were prepared with deionized water (except for CAL and IVM, which where dissolved in ethanol and dimethyl sulphoxide (DMSO) respectively), aliquots thereof were stored at –20°C, and the ultimate dilutions were made daily with the appropriate extracellular saline. For DMSO, as well as ethanol, the final content in the bath never exceeded 0.3%, a quantity lacking in both cases any effect on ATP-induced currents in astroglial cells ($n = 7$ each, $N = 1–2$). All solutions were routinely checked for acidification caused by added ATP or its structural analogues, and, if necessary (usually for concentration > 100 μM), readjusted to the desired pH value.

Statistics

Results are expressed throughout as means ± SEM obtained in n cells from N different preparations. Differences between means were tested for significance (SigmaStat, version 3.5, Systat Software Inc) by the Mann–Whitney U-test or by the Kruskall–Wallis one-way ANOVA on ranks followed by a modified t-test (Bonferroni–Dunn) in the case of single and multiple comparisons respectively. $P < 0.05$ was the accepted minimum level of significance.

Results

Cell selection and general observations

Presumed astrocytes were selected under phase contrast optics based on morphological criteria. They formed a more or less confluent background layer of greyish flat cells, which were devoid of clearly circumscribable single-cell borders and appendages (Figure 1A). It should be noted that the vast majority of these carpet-forming cells stained positive for the astrocytic marker GFAP (Fischer *et al*., 2009). The appearance of presumed astrocytes was, thus, clearly different from that of cortical neurones, which were characterized by a phase contrast-bright halo around their cell bodies and which had developed long network-forming dendrite-like processes after 12–16 days *in vitro* (Figure 1A).

The presumed astrocytes were electrophysiologically heterogeneous; three different membrane current patterns in response to a voltage-step protocol could be observed. Cells showed either strong outward rectification (Figure 1B), an intermediate (variably) rectifying phenotype (Figure 1D), or almost symmetrical, largely time- and voltage-independent (passive) responses to de- and hyperpolarizing voltage

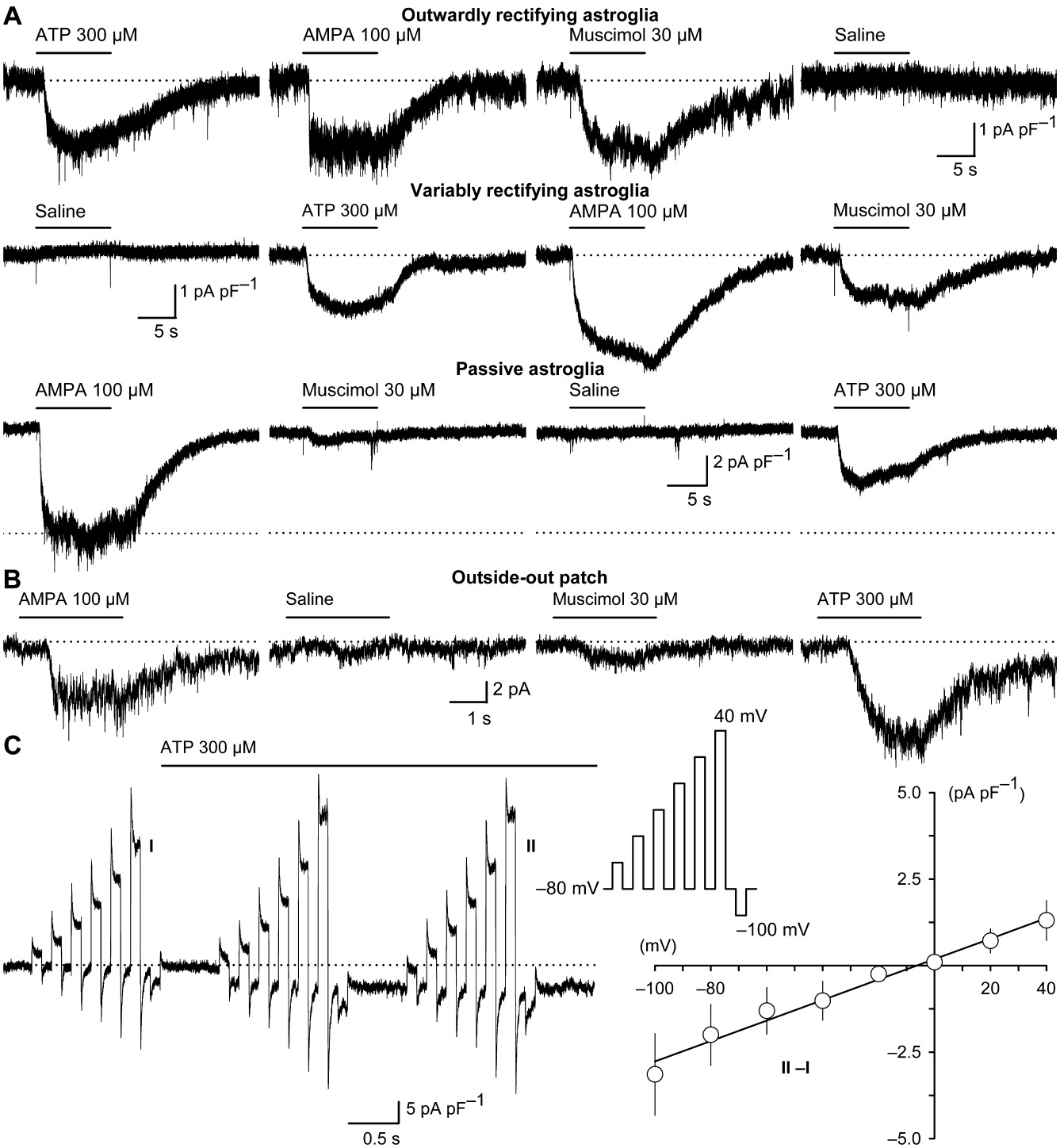

Figure 2 Evidence for P2X receptors in rat cultured cortical astroglia. (A) Shown are, from top to bottom, inward current responses to ATP (300 μM) and drug-free bath solution (saline) in an outwardly rectifying, a variably rectifying and a passive rat cortical astroglial cell (compare Figure 1). Also shown are the effects of AMPA (100 μM) and muscimol (30 μM), which were used for comparison. Agonists were applied for 10 s. The holding potential was −80 mV, and the standard bath and K^+-based pipette solution were used. Individual challenges with the agonists were interspersed by 4 min superfusion periods with drug-free saline. (B) Inward currents evoked by ATP and drug-free bath solution, as well as by AMPA and muscimol in an outside-out patch excised from an astroglial cell; same protocol as in (A), except that agonist application was for 3 s. (C) Characterization of the ATP-induced conductance. Repetitive cycles of short voltage steps (100 ms in duration, one step every 100 ms from a holding potential of −80 mV to various test potentials; for pattern see inset) were applied to construct *I-V* curves for the ATP (300 μM)-induced current. To study the effects of ATP in more isolation, a Cs^+-based pipette solution was used to block part of the astroglial cell K^+ conductance. The left panel shows a representative whole-cell recording obtained under these conditions. The net ATP-induced current was then derived by subtracting the current amplitudes (measured at the end of the voltage steps) recorded before (I) from those recorded 2.6 s after the ATP application had started (II). The *I-V* graph (II–I, right panel) represents data from eight cells ($N = 2$).

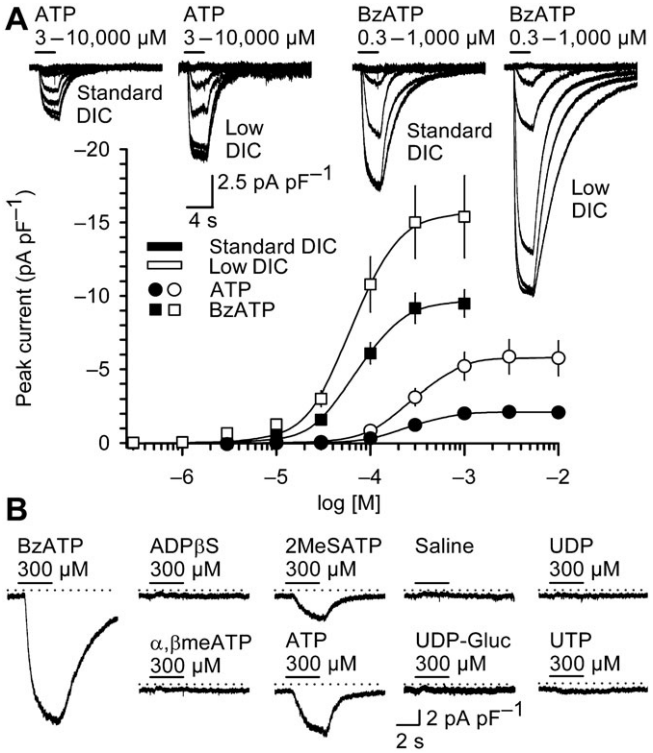

Figure 3 Effects of extracellular divalent cations (DICs) on P2X receptor agonist potencies as well as effects of various P2X and P2Y receptor agonists in rat cultured cortical astroglia. (A) Concentration-response curves for the peak currents induced by ATP (3–10 000 μM) and 2′-3′-O-(4-benzoyl) ATP (BzATP) (0.3–1000 μM) in rat cortical astrocytes recorded either with standard concentrations of extracellular DICs (standard DIC; 1.2 mM Mg^{2+} and 1.0 mM Ca^{2+}) or in a low DIC-containing bath (low DIC; 0 mM added Mg^{2+}, 0.1 mM Ca^{2+}). The continuous lines were obtained by fitting a three-parameter logistic function (Hill equation) to the averaged data (n = 9–13, N = 3–4). Concentration-response curves were constructed from currents in response to subsequently increasing drug concentrations, pressure applied for 3 s at a holding potential of −80 mV, which were separated by a 4 min washout with the respective agonist-free bath solutions (standard bath or low DIC). The insets show, from left to right, representative superimposed whole-cell currents evoked by increasing concentrations of ATP in standard DIC, ATP in low DIC, BzATP in standard DIC and BzATP in low DIC. (B) Representative whole-cell currents evoked by 300 μM of BzATP, adenosine 5′-O-(2-thiodiphosphate) (ADPβS), 2-(methylthio) ATP (2MeSATP), drug-free bath solution (saline), uridine 5′-diphosphate (UDP), α,β-methylene ATP (α,βmeATP), ATP, uridine 5′-diphosphoglucose (UDP-Gluc) and uridine 5′-triphosphate (UTP) in a rat cortical astroglial cell. P2 agonists were consecutively applied (for 3 s every 4 min at a holding potential of −80 mV) to the same set of cells. The order of agonist application was varied between individual trials. As in (A), a Cs^+-based pipette solution was used. The bath solution was low DIC to allow for the detection of even small events.

commands (Figure 1F). In the outwardly rectifying cells, depolarization-activated transient inward currents preceded the outward currents (inset Figure 1B). These inward currents were blocked by TTX (0.3 μM) and were, hence, Na^+ currents (data not shown).

Most importantly, immunoreactivity for the astrocytic marker GFAP was, regardless of the particular current profile observed, always detectable in a sample of LY-filled cells (n = 14, N = 6; Figure 1C,E,G), thereby authenticating their astrocyte identity, as well as the reliability of the visual cell type identification. Moreover, the standard 15 min pretreatment of cultures with CBX (100 μM) had quite effectively occluded gap junctional coupling (Murphy *et al*., 1993) because LY diffusion could be verified only in one presumed astrocyte, which was coupled to four neighbouring glial cells (not shown). In all other cases, only one Hoe-positive cell nucleus was co-localized with the LY- and GFAP staining (Figure 1C,E,G). By comparison, 70–100% of the different astrocyte types in hippocampal brain slices showed syncytial coupling in the absence of gap junction blockade (Schools *et al*., 2006). It should be noted in addition that the cultured glial cells extended from the GFAP-positive somata a meshwork of fine, LY-filled appendages (e.g. Figure 1C), not visible under conventional phase contrast optics (e.g. Figure 1A). Thus, they shared, albeit on a two-dimensional array, apparently some structural similarities with their astrocytic counterparts in the brain. Despite these obvious conformities, divergences between the properties of astrocytes *in situ* and those grown in culture may also exist. The term astroglia, hence, will be used throughout for our cultured cortical astrocyte-like cells, just to indicate this point.

Presence of functional P2X receptors in rat cultured cortical astroglia

Next, we explored the presence of P2X receptors in the electrophysiologically differing astroglial phenotypes. From a total of 70 cells (N = 19) investigated in this set of experiments, 23% displayed an outwardly rectifying, 31% a variably rectifying and 46% a passive membrane current profile. However, in every cell of this survey, irrespective of the voltage-dependent current pattern each actually displayed, ATP (300 μM) evoked whole-cell inward currents (Figure 2A; −5.1 ± 0.3 pA·pF^{-1}), which were significantly different from the effects of bath solution alone (0.0 ± 0.2 pA·pF^{-1}; P < 0.05). For comparison, the prototypical ionotropic glutamate and $GABA_A$ receptor agonists AMPA (100 μM) and muscimol (30 μM) were also applied to the same cells (Figure 2A). The currents evoked were −7.5 ± 0.9 pA·pF^{-1} and −3.5 ± 0.3 pA·pF^{-1}, respectively, both being significantly different from the bath solution-induced changes (P < 0.05).

Of course, the currents in response to ATP could have been mediated by an indirect action, such as by inducing the release of mediators such as glutamate from cells located in the neighbourhood of the astroglia under investigation. To account for this possibility, we prepared excised outside-out patch vesicles and lifted them approximately 200 μm above the cell layer before they were challenged with ATP. The P2 receptor agonist (300 μM) was, however, still able to elicit inward currents, even under these conditions (Figure 2B; −9.3 ± 2.0 pA). The nucleotide-evoked responses, moreover, were again significantly different from the effects of pressure-applied saline (0.4 ± 1.2 pA; P < 0.05; n = 7, N = 2). Under the same conditions, AMPA (100 μM; −10.8 ± 2.4 pA) and muscimol (30 μM; −9.2 ± 2.2 pA) also caused current responses in each of the isolated patch vesicles, which significantly differed from the effect of the batch solution alone (P < 0.05).

The ATP (300 μM)-induced whole-cell currents reversed sign at −5.1 ± 4.3 mV, a reversal potential close to the theoretical equilibrium potentials for a non-selective cationic

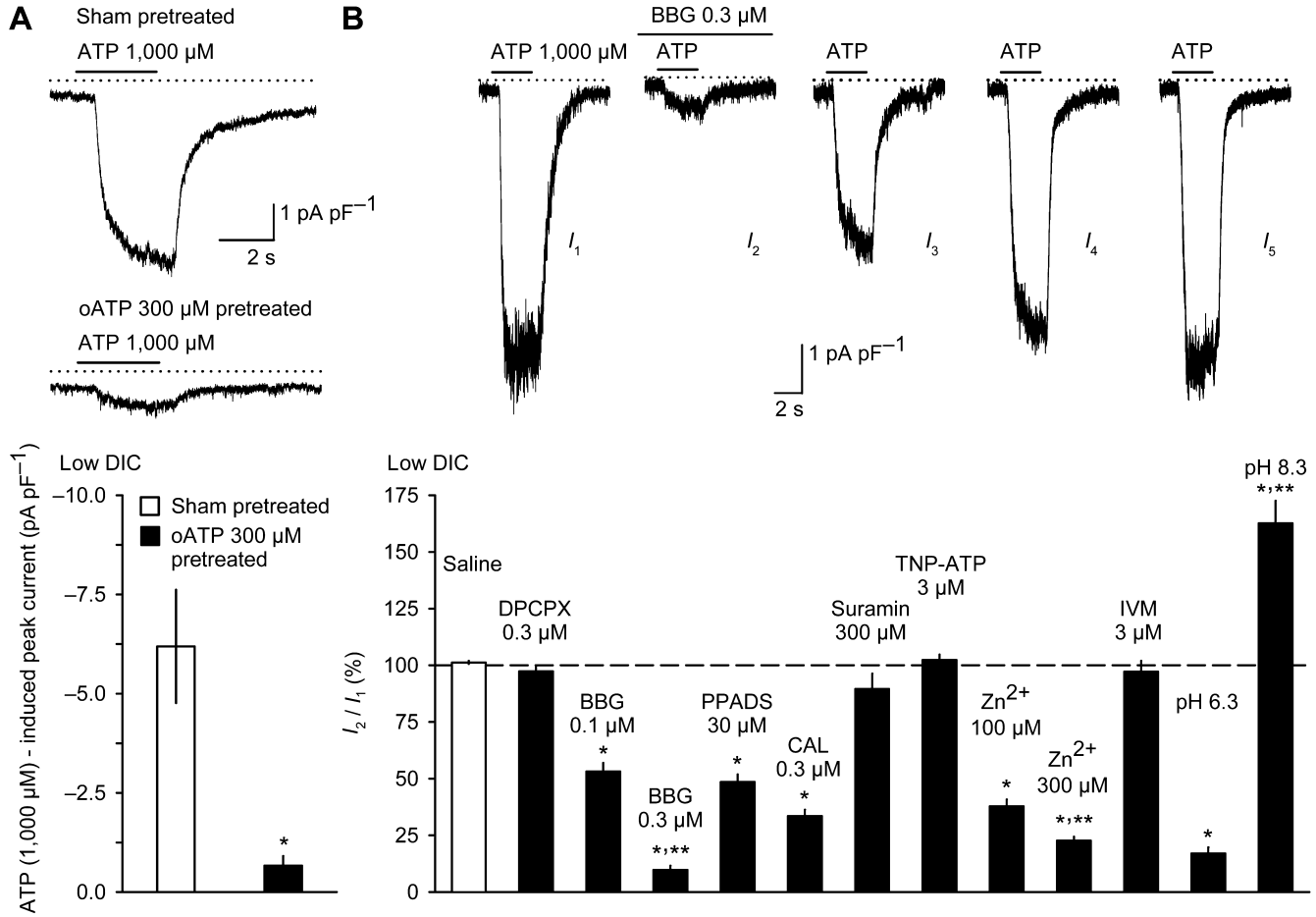

Figure 4 Effects of antagonists and modulators on P2X receptors in rat cultured cortical astroglia. (A) Two representative whole-cell currents evoked in response to ATP (1000 μM for 3 s at a holding potential of –80 mV) in a control astroglial cell (upper panel, sham pretreated) and in an astroglial cell pretreated with the irreversible P2X7 receptor antagonist ATP periodate oxidized (oATP; 300 μM; lower panel). Cells were exposed to a culture medium containing either no oATP or 300 μM of the antagonist for a 3 h period in the incubator. Then, cells were washed thoroughly with drug-free medium and incubated for another 3–6 h before the experiments were initiated. The histogram beneath the current traces represents the results from 10 similar experiments in sham- and oATP-pretreated cells, respectively ($N = 3$ each). *$P < 0.05$, significant difference between the effects of ATP in sham-pretreated and oATP-pretreated astrocytes. (B) Upper panel, whole-cell currents in response to five subsequent applications (I_1–I_5) of ATP (1000 μM for 3 s at –80 mV) spaced by 4 min intervals. The P2X7 receptor antagonist Coomassie Brilliant Blue G (BBG; 0.3 μM) was present in the superfusion medium for the 4 min before and during I_2. As in (A), a Cs^+-based pipette solution was used, and the bath was low DIC to augment the otherwise rather small nucleotide responses. The histogram beneath the current traces summarizes the data derived from similar interaction experiments. The only procedural exception was Zn^{2+} (zinc), which was directly co-applied with ATP at I_2. Shown are the effects of the drug-free bath solution (saline), of the adenosine receptor antagonist 1,3-dipropyl-8-cyclopentylxanthine (DCPCX; 0.3 μM), of the P2X receptor antagonists BBG (0.1 and 0.3 μM), pyridoxal-5′-phosphate-6-azophenyl-2′,4′-disulphonic acid (PPADS; 30 μM), calmidazolium (CAL; 0.3 μM), suramin (300 μM) and 2′-3′-O-(2,4,6-trinitrophenyl) ATP (TNP-ATP; 3 μM), and of the P2X receptor modulators Zn^{2+} (100 and 300 μM) and ivermectin (IVM, 3 μM), as well as those induced by acidification (pH 6.3) or alkalinization (pH 8.3) of the bath [$n = 31$, $N = 24$ for controls (saline) and $n = 7$–9, $N = 2$ each for experiments with antagonist and modulators]. The columns represent the ratio of I_2 with respect to I_1 expressed as percentage of I_1. *$P < 0.05$, significant differences from the effects of drug-free bath solution (saline); **$P < 0.05$, significant differences from the effects of BBG 0.1 μM, Zn^{2+} 100 μM or pH 6.3 respectively.

conductance (0 mV). The conductance increase was thereby almost linear over a broad voltage range (Figure 2C). It averaged 32.6 ± 12.5 pS·pF^{-1} ($n = 8$, $N = 2$). Thus, in the astrocytes investigated, ATP had activated non-selective cation channels, that is, typical P2X receptors. Similarly, non-selective cation channels gated by AMPA as well as chloride channels gated by GABA appear also to be present in the same astrocytes.

Subtype determination of rat cultured cortical astroglial P2X receptors by agonists

In order to gain a more detailed information about the P2X receptor subtype(s) involved in the actions of ATP, we next compared its effects with those of BzATP, which is in fact a substantially more potent agonist at P2X1, P2X3, P2X7, P2X1/2 and P2X4/7 receptors. Within this group, P2X7 is, however, the least sensitive subtype, with reported EC_{50} values for recombinant receptors around 20 and 100 μM for BzATP and ATP, respectively (Jarvis and Khakh, 2009). As current flow through P2X2 and P2X7 receptors was inhibited by extracellular DICs (Jarvis and Khakh, 2009), experiments were repeated in a low DIC-containing bath (low DIC; 0 Mg^{2+} and 0.1 mM Ca^{2+}).

ATP and BzATP caused, in a concentration-dependent manner, inward currents in all 48 cortical astroglial cells challenged in this way. Under standard extracellular conditions

(1.2 Mg^{2+} and 1.0 mM Ca^{2+}, respectively), ATP started to act at concentrations ≥30 μM. The concentration-response curve for the nucleotide levelled off to an extrapolated maximum of –2.1 pA·pF^{-1} at about 3000 μM. It had an EC_{50} of 251 μM, and the Hill coefficient was 1.9 (Figure 3A; n = 13, N = 4). The threshold concentration, EC_{50} value (279 μM), slope (1.8) and inflexion towards the plateau were similar in low DIC. The maximum ATP effect was, however, more than twofold in these experiments (–5.8 pA·pF^{-1}; Figure 3A; n = 13, N = 4). The concentration-response curves for BzATP, however, started one log unit below that of ATP at concentrations of ≥3 μM, had already reached their plateau at about 300 μM, had more than threefold lower EC_{50} values of 74 and 64 μM, and had Hill slopes of 1.8 and 1.7 in standard DIC and low DIC respectively. Their maxima were –9.7 pA·pF^{-1} in standard DIC and –15.8 pA·pF^{-1} in low DIC, and, hence, approximately threefold greater than those which were achieved by ATP under the respective conditions (Figure 3A; n = 9 and 13, N = 3 and 4).

Next, we compared the effects of ATP with those of two additional P2X receptor agonists. These were α,βmeATP, active at P2X1, P2X3, P2X6, P2X1/2, P2X1/4, P2X1/5, P2X2/3, P2X2/6 and P2X4/6 receptors, and 2MeSATP, which may, like ATP, stimulate all hitherto known homomeric, as well heteromeric P2X subtypes (Jarvis and Khakh, 2009). It should be remembered, however, that ATP ($P2Y_2$, $P2Y_4$ and $P2Y_{12}$), BzATP ($P2Y_2$) and 2MeSATP ($P2Y_1$ and $P2Y_6$) also displayed considerable agonistic properties at rat G protein-coupled P2Y receptors (von Kügelgen, 2006). Therefore, in addition, we explored the possible effects of the P2Y receptor selective agonists ADPβS ($P2Y_1$, $P2Y_{12}$ and $P2Y_{13}$), UTP ($P2Y_2$ and $P2Y_4$), UDP ($P2Y_6$) and UDP-Gluc ($P2Y_{14}$; von Kügelgen, 2006).

Of the eight agonists tested, only ATP, BzATP and 2MeSATP evoked inward currents clearly different from the effects of pressure-applied drug-free low DIC (P < 0.05; Figure 3B; n = 12, N = 3). The currents induced by ATP (–4.3 ± 1.0 pA·pF^{-1}) and 2MeSATP (–2.2 ± 0.3 pA·pF^{-1}) were thereby similar in amplitude (P > 0.05) but differed significantly from those evoked by BzATP (P < 0.05; –12.9 ± 1.9 pA·pF^{-1}).

The inability of ADPβS, UTP, UDP and UDP-Gluc to cause an effect, together with the suppression of ATP- and BzATP-activated currents by physiological concentrations of extracellular DICs, was again compatible with the functional presence of P2X receptors in our astroglial cells. As P2X5 is insensitive to BzATP, and as P2X1,3,6 homotrimeric and P2X1/2,1/4,1/5,2/3,2/6,4/6 heterotrimeric receptors should have been activated by the high concentration of α,βmeATP (300 μM) used, the remaining possibilities were P2X2, P2X4, P2X7 and P2X4/7 (Jarvis and Khakh, 2009). However, the overall low sensitivity to nucleotides, as indicated by the rather high EC_{50} values for ATP and BzATP, as well as the higher potency (EC_{50}) and efficacy (maximum effect) of BzATP in comparison with ATP, suggested that P2X7 receptors were involved.

Subtype determination of rat cultured cortical astroglial P2X receptors by antagonists and modulators

Next, we investigated the effects of oATP on the ATP-induced currents in our cortical astroglia. This compound has been characterized previously as an irreversible antagonist at P2X7 receptors that also blocks P2X1 and P2X2 receptors at similar concentrations (100–300 μM), albeit in a reversible manner (within 15–25 min after washout; Evans *et al*., 1995). The currents evoked by an approximate EC_{90} of ATP (1000 μM), remaining after pretreatment with oATP (300 μM) and an additional washout period of 3–6 h, were in fact only ~10% of that measured in respective controls (Figure 4A; n = 10 each, N = 3 each).

The actions of all other antagonists and modulators were then evaluated in direct interaction experiments. It should be noted that the adenosine receptor antagonist DPCPX (0.3 μM) did not interfere with ATP (1000 μM), thereby excluding any major involvement of the ATP-hydrolysis product adenosine in the response (Figure 4B). The P2X7 receptor antagonists tested in addition were BBG, at concentrations of <1000 μM selective for this receptor subtype (Jiang *et al*., 2000), PPADS with known antagonistic properties at all homomeric P2X receptors except P2X4 (Jarvis and Khakh, 2009), and CAL, an inhibitor of Ca^{2+}/calmodulin-dependent protein kinase II that also displays potent P2X7 antagonistic effects (Virginio *et al*., 1997). Suramin, lacking inhibitory properties at rat P2X7 and having, in addition, a spectrum of antagonistic activities similar to that of PPADS (Jarvis and Khakh, 2009), was used as a negative control. The functional presence of P2X4/7 heteromeric receptors was, eventually, investigated by the antagonist TNP-ATP (Guo *et al*., 2007), a compound that also suppresses effects mediated by P2X1–4, P2X1/4, P2X1/5 and P2X2/3 (Jarvis and Khakh, 2009).

BBG (0.1 and 0.3 μM; n = 8 each, N = 2 each) significantly inhibited the ATP (1000)-induced currents in a concentration-dependent manner (Figure 4B). This inhibition was, in line with previous observations (Jiang *et al*., 2000), only slowly reversible (Figure 4B). PPADS (30 μM) and CAL (0.3 μM; n = 7, N = 2 each) also depressed the ATP effects by approximately 50 and 60%, whereas suramin (300 μM; n = 8, N = 2) and TNP-ATP (3 μM; n = 9, N = 2) were ineffective (Figure 4B).

These data strongly argued against the functional presence of P2X2 and P2X4/7. P2X2 receptors are highly sensitive to PPADS, suramin and TNP-ATP with IC_{50} values of 1 μM (PPADS and TNP-ATP) and 10 μM (suramin), and the estimated IC_{50} of TNP-ATP at P2X4/7 heteromers is, likewise, between 1 μM and 2 μM (Guo *et al*., 2007; Jarvis and Khakh, 2009).

Rat P2X4 homomeric receptors are, however, admittedly resistant to the inhibitory actions of all common P2X receptor antagonists (Jarvis and Khakh, 2009). In order to dispel any remaining ambiguities, we therefore performed additional experiments with the P2X receptor modulators Zn^{2+}, protons (pH 6.3 instead of 7.3) and IVM. Zn^{2+} has been reported to potentiate currents through P2X2 and P2X4 receptors (Garcia-Guzman *et al*., 1997; Wildman *et al*., 1998). At P2X4, the Zn^{2+} concentration-response curve is, however, bell shaped, displaying its maximum at about 10 μM, whereas its potentiating effects vanish at about 100 μM and then turn into profound inhibition at still higher concentrations (Garcia-Guzman *et al*., 1997). At P2X7 receptors, in contrast, Zn^{2+} only inhibits BzATP-induced currents, and this has been observed at ≥1 μM (Virginio *et al*., 1997). Ambient acidification to a pH of 6.3, however, exclusively amplifies P2X2

receptor-mediated currents (Stoop *et al*., 1997), whereas those mediated through P2X4 and P2X7 receptor channels are substantially suppressed (Stoop *et al*., 1997; Virginio *et al*., 1997). IVM is a positive allosteric modulator of P2X4 (Khakh *et al*., 1999) and P2X4/7 (Guo *et al*., 2007) but has little effect on the remaining subtypes of homomeric or heteromeric P2X receptors (Jarvis and Khakh, 2009).

Zn^{2+} (100 and 300 μM; n = 7–8, N = 2 each) significantly inhibited the ATP (1000)-induced currents in rat cortical astroglia in a concentration-dependent manner (Figure 4B). Lowering the extracellular pH to 6.3 (n = 9, N = 2) produced, likewise, marked inhibition (Figure 4B). This was most unlikely to be due to cellular damage caused by a 4 min exposure to the acidic solution because alkalinization to a pH of 8.3 (n = 9, N = 2) had the opposite effect. Compared with controls, the ATP-induced currents under these conditions were potentiated by approximately 60% (Figure 4B). IVM (3 μM; n = 7, N = 2) failed to modulate the currents evoked by ATP (Figure 4B). Thus, P2X7 is the predominant P2X receptor subtype functionally expressed in rat cultured cortical astroglia.

Discussion

The electrophysiological characteristics (outwardly rectifying, variably rectifying or passive; see Figure 1) of the rat cultured astroglia investigated in this study closely resembled those of astrocytes in neocortical brain slices, although similar current profiles have also been identified in such cells from many other regions of the rat brain (Bordey and Sontheimer, 2000; Zhou *et al*., 2006).

In accordance with our previous immunohistochemical detection of the particular protein (Fischer *et al*., 2009), we have now functionally identified P2X7 receptors on rat neocortical astroglia as potential targets for ATP. The main arguments for this diagnosis were: (i) a reversal potential of ATP-induced currents near to that expected for non-selective cationic channels (0 mV); (ii) a higher potency of BzATP in comparison with that of ATP itself, in combination with an overall low sensitivity to these nucleotides, as well as the large increase in efficacy of the two agonists in a low DIC bath medium; (iii) the lack of effect of non-P2X7/P2Y subtype specific agonists (α,βmeATP, ADPβS, UTP, UDP and UDP-Gluc); and, eventually, (iv) the inhibition of ATP-induced currents by subtype selective antagonists (oATP, BBG and CAL) and allosteric modulators (Zn^{2+} and protons).

Our data agree with previous work that has also provided electrophysiological evidence for the presence of functional P2X7 receptors in astrocytes from cortical cell cultures from mice (Duan *et al*., 2003), as well as hippocampal brain slices from rats (Fellin *et al*., 2006). However, controversial observations also exist. In hippocampal brain slices from transgenic mice, where astrocytes were identified by human GFAP promoter-controlled expression of enhanced green fluorescent protein (Tg(hGAFP/EGFP)), no P2X receptor-mediated currents could be recorded (Jabs *et al*., 2007). Moreover, acutely dissociated cortical astrocytes from the same mouse line were undeniably endowed with functional P2X receptors, albeit with properties of P2X1/5 heteromers (Lalo *et al*., 2008). However, for the most of the experiments on brain slices (Jabs *et al*., 2007), rather low concentrations of agonists were used (ATP 100 μM; BzATP 20 μM), which may be subthresholds for the activation of P2X7 receptors (compare with Figure 3A). Shortly after mechanical dissociation (Lalo *et al*., 2008), however, profound actin cytoskeleton reorganization may occur in astrocytes (DeMali *et al*., 2003) interfering with the otherwise tight association of P2X7 receptors with the actin cytoskeleton (Kim *et al*., 2001) and, thus, possibly also with their membrane insertion. Hence, it is still quite possible that P2X7, indeed, constitutes the major P2X subunit functionally expressed in astrocytes.

ATP may be released from axon terminals during synaptic transmission, as well as from neighbouring glial cells (Araque *et al*., 1999; Burnstock, 2007). In addition, ATP poured out by damaged astrocytes or neurones during brain injury may also activate these P2X7 receptors (Franke and Illes, 2006). Hence, the question arises as to the purpose of these receptors. Astrocyte P2X7 receptors have been suggested to mediate physiological glia–neurone communication by providing an ATP-gated release pathway for gliotransmitter glutamate (Duan *et al*., 2003; Fellin *et al*., 2006). However, in view of the very large amounts of nucleotide needed to activate these receptors, we favour the idea that coexisting G protein-coupled P2 receptors, for example, $P2Y_1$, $P2Y_2$ and $P2Y_4$ (Fischer *et al*., 2009), constitute more appropriate targets for physiological crosstalk tasks instead. In fact, ATP at P2Y receptors (especially $P2Y_{1,2}$) has been shown to evoke the propagation of Ca^{2+} waves (Fam *et al*., 2003), considered to be the primary manifestation of cell-to-cell communication among astrocytic networks (Araque *et al*., 1999; 2001; Burnstock, 2007). We have proposed, based on *in situ* recordings of NMDA receptor currents from pyramidal neurones of rodent prefrontal cortical slices, that $P2Y_4$ receptors release glutamate from astrocytes, which in turn may facilitate neuronal NMDA receptors *via* the activation of metabotropic glutamate receptors (Wirkner *et al*., 2007). In fact, a Ca^{2+}-dependent vesicular release of glutamate from astrocytes in response to various neurotransmitter molecules including ATP has been repeatedly demonstrated (Parpura *et al*., 1994; Jeremic *et al*., 2001).

However, under pathophysiological conditions, the glial P2X7 receptors may gain increased functionality, as, for example, alkalinization markedly potentiated their effects (Figure 4B). In a rat model of febrile seizures, the most common type of convulsions that occurs in humans during early childhood, ictal activity was preceded by a pronounced rise in breathing rate that caused respiratory alkalosis and concomitantly enhanced neuronal activity (Schuchmann *et al*., 2006). Gliotransmitter glutamate has been shown, however, to be involved in the generation of convulsive activity (Tian *et al*., 2005). Thus, glutamate release through astrocyte P2X7 receptors (Duan *et al*., 2003; Fellin *et al*., 2006) may be involved in triggering various types of seizure events. In addition, the increased sensitivity of P2X7 receptors to ATP in a low DIC-containing external medium, which is a well-known manoeuvre to induce epileptic activity, for example, in hippocampal pyramidal neurones, also suggests the participation of this receptor class in CNS convulsions (Heinemann *et al*., 1992; Franke and Illes, 2006).

Whereas normal neuro- or gliotransmission fails to generate high local concentrations of ATP in the extracellular space, pathophysiological events may do so via a massive efflux of intracellular ATP from metabolically compromised or otherwise damaged CNS neurones and astrocytes, resulting in apoptotic/necrotic or proliferative reactions (Franke and Illes, 2006). Under *in vivo* conditions, mechanical (Franke *et al*., 2001) or ischaemic injury (Collo *et al*., 1997; Franke *et al*., 2004) has been shown to initiate the expression of previously absent P2X7 receptor immunoreactivity on microglia, astrocytes and neurones. Oxygen/glucose deprivation, moreover, up-regulated P2X7 receptor immunoreactivity in primary cultures of cerebellar granule neurones (Cavaliere *et al*., 2002) and in CA1 pyramidal neurones of organotypical hippocampal cultures (Cavaliere *et al*., 2004). Hence, it has been hypothesized that the excessive outflow of ATP causes up-regulation of neuronal and glial P2X7 receptors, and, thereby, aggravates the cellular necrosis caused by the injury itself.

Although the present study supports the presence of P2X7 receptors at astrocytes, it does not exclude the existence of such receptors at neurones. Both immunohistochemistry and functional data have strongly suggested that, for example, cerebellar granule neurones (Cavaliere *et al*., 2002; León *et al*., 2008), hippocampal CA1 pyramidal cells (Cavaliere *et al*., 2004), and, at presynaptic sites, cerebrocortical interneurones (Wirkner *et al*., 2005) are also endowed with P2X7 receptors. Previously, immunohistochemistry studies have questioned the selectivity of receptor antibodies as reliable markers of P2X7 receptors, and, hence, it was concluded that these receptors are probably absent at any type of neurone in the CNS (Sim *et al*., 2004). However, more recent studies strongly suggest that this assumption does not hold true (Sánchez-Nogueiro *et al*., 2005; Nicke *et al*., 2009; see Sperlágh *et al*., 2006).

Acknowledgements

This work was supported by the Deutsche Forschungsgemeinschaft, Bonn (IL 20/16-1).

Conflicts of interest

None.

References

Alexander SPH, Mathie A, Peters JA (2009). Guide to receptors and channels (GRAC), 4th edn. *Br J Pharmacol* **158** (Suppl. 1): S1–S254.

Araque A, Carmignoto G, Haydon PG (2001). Dynamic signaling between astrocytes and neurons. *Annu Rev Physiol* **63**: 795–813.

Araque A, Parpura V, Sanzgiri RP, Haydon PG (1999). Tripartite synapses: glia, the unacknowledged partner. *Trends Neurosci* **22**: 208–215.

Barry PH (1994). JPCalc, a software package for calculating liquid junction potential corrections in patch-clamp, intracellular, epithelial and bilayer measurements and for correcting junction potential measurements. *J Neurosci Methods* **51**: 107–116.

Bordey A, Sontheimer H (2000). Ion channel expression by astrocytes in situ: comparison of different CNS regions. *Glia* **30**: 27–38.

Burnstock G (2007). Physiology and pathophysiology of purinergic neurotransmission. *Physiol Rev* **87**: 659–797.

Cavaliere F, Amadio S, Sancesario G, Bernardi G, Volonté C (2004). Synaptic $P2X_7$ and oxygen/glucose deprivation in organotypic hippocampal cultures. *J Cereb Blood Flow Metab* **24**: 392–398.

Cavaliere F, Sancesario G, Bernardi G, Volonté C (2002). Extracellular ATP and nerve growth factor intensify hypoglycemia-induced cell death in primary neurons: role of P2 and NGFRp75 receptors. *J Neurochem* **83**: 1129–1138.

Collo G, Neidhart S, Kawashima E, Kosco-Vilbois M, North RA, Buell G (1997). Tissue distribution of the $P2X_7$ receptor. *Neuropharmacology* **36**: 1277–1283.

DeMali KA, Wennerberg K, Burridge K (2003). Integrin signaling to the actin cytoskeleton. *Curr Opin Cell Biol* **15**: 572–582.

Duan S, Anderson CM, Keung EC, Chen Y, Chen Y, Swanson RA (2003). $P2X_7$ receptor-mediated release of excitatory amino acids from astrocytes. *J Neurosci* **23**: 1320–1328.

Evans RJ, Lewis C, Buell G, Valera S, North RA, Surprenant A (1995). Pharmacological characterization of heterologously expressed ATP-gated cation channels (P_{2x} purinoceptors). *Mol Pharmacol* **48**: 178–183.

Fam SR, Gallagher CJ, Kaila LV, Salter MW (2003). Differential frequency dependence of $P2Y_1$- and $P2Y_2$-mediated Ca^{2+} signaling in astrocytes. *J Neurosci* **23**: 4437–4444.

Fellin T, Pozzan T, Carmignoto G (2006). Purinergic receptors mediate two distinct glutamate release pathways in hippocampal astrocytes. *J Biol Chem* **281**: 4274–4284.

Fischer W, Appelt K, Grohmann M, Franke H, Nörenberg W, Illes P (2009). Increase of intracellular Ca^{2+} by P2X and P2Y receptor-subtypes in cultured cortical astroglia of the rat. *Neuroscience* **160**: 767–783.

Fischer W, Franke H, Appelt K, Schunk J, Sobottka H, Illes P *et al*. (2008). Evidence of various functional P2Y as well as $P2X_7$ nucleotide receptors in cultured cerebrocortical astrocytes of the rat. *Naunyn Schmiedeberg's Arch Pharmacol* **377**: 20.

Franke H, Grosche J, Schädlich H, Krügel U, Allgaier C, Illes P (2001). P2X receptor expression on astrocytes in the nucleus accumbens of rats. *Neuroscience* **108**: 421–429.

Franke H, Günther A, Grosche J, Schmidt R, Rossner S, Reinhardt R *et al*. (2004). $P2X_7$ receptor expression after ischemia in the cerebral cortex of rats. *J Neuropathol Exp Neurol* **63**: 686–699.

Franke H, Illes P (2006). Involvement of P2 receptors in the growth and survival of neurons in the CNS. *Pharmacol Ther* **109**: 297–324.

Fumagalli M, Brambilla R, D'Ambrosi N, Volonté C, Matteoli M, Verderio C *et al*. (2003). Nucleotide-mediated calcium signaling in rat cortical astrocytes: role of P2X and P2Y receptors. *Glia* **43**: 218–230.

Garcia-Guzman M, Soto F, Gomez-Hernandez JM, Lund PE, Stühmer W (1997). Characterization of recombinant human $P2X_4$ receptor reveals pharmacological differences to the rat homologue. *Mol Pharmacol* **51**: 109–118.

Guo C, Masin M, Qureshi OS, Murrell-Lagnado RD (2007). Evidence for functional $P2X_4/P2X_7$ heteromeric receptors. *Mol Pharmacol* **72**: 1447–1456.

Heinemann U, Albrecht D, Köhr G, Rausche G, Stabel J, Wisskirchen T (1992). Low-Ca^{2+}-induced epileptiform activity in rat hippocampal slices. *Epilepsy Res Suppl* **8**: 147–155.

Jabs R, Matthias K, Grote A, Grauer M, Seifert G, Steinhäuser C (2007). Lack of P2X receptor mediated currents in astrocytes and GluR type glial cells of the hippocampal CA1 region. *Glia* **55**: 1648–1655.

Jarvis MF, Khakh BS (2009). ATP-gated P2X cation-channels. *Neuropharmacology* **56**: 208–215.

Jeremic A, Jeftinija K, Stevanovic J, Glavaski A, Jeftinija S (2001). ATP stimulates calcium-dependent glutamate release from cultured astrocytes. *J Neurochem* **77**: 664–675.

Jiang LH, Mackenzie AB, North RA, Surprenant A (2000). Brilliant blue G selectively blocks ATP-gated rat $P2X_7$ receptors. *Mol Pharmacol* **58**: 82–88.

Khakh BS, Proctor WR, Dunwiddie TV, Labarca C, Lester HA (1999). Allosteric control of gating and kinetics at $P2X_4$ receptor channels. *J Neurosci* **19**: 7289–7299.

Kim M, Jiang LH, Wilson HL, North RA, Surprenant A (2001). Proteomic and functional evidence for a $P2X_7$ receptor signalling complex. *EMBO J* **20**: 6347–6358.

Lalo U, Pankratov Y, Wichert SP, Rossner MJ, North RA, Kirchhoff F *et al*. (2008). $P2X_1$ and $P2X_5$ subunits form the functional P2X receptor in mouse cortical astrocytes. *J Neurosci* **28**: 5473–5480.

León D, Sánchez-Nogueiro J, Marín-García P, Miras-Portugal MA (2008). Glutamate release and synapsin-I phosphorylation induced by P2X7 receptors activation in cerebellar granule neurons. *Neurochem Int* **52**: 1148–1159.

Murphy TH, Blatter LA, Wier WG, Baraban JM (1993). Rapid communication between neurons and astrocytes in primary cortical cultures. *J Neurosci* **13**: 2672–2679.

Nicke A, Kuan YH, Masin M, Rettinger J, Marquez-Klaka B, Bender O *et al*. (2009). A functional $P2X_7$ splice variant with an alternative transmembrane domain 1 escapes gene inactivation in $P2X_7$ knockout mice. *J Biol Chem* **284**: 25813–25822.

Nobile M, Monaldi I, Alloisio S, Cugnoli C, Ferroni S (2003). ATP-induced, sustained calcium signalling in cultured rat cortical astrocytes: evidence for a non-capacitative, P2X7-like-mediated calcium entry. *FEBS Lett* **538**: 71–76.

Parpura V, Basarsky TA, Liu F, Jeftinija K, Jeftinija S, Haydon PG (1994). Glutamate-mediated astrocyte-neuron signalling. *Nature* **369**: 744–747.

Sánchez-Nogueiro J, Marín-García P, Miras-Portugal MT (2005). Characterization of a functional $P2X_7$-like receptor in cerebellar granule neurons from $P2X_7$ knockout mice. *FEBS Lett* **579**: 3783–3788.

Schools GP, Zhou M, Kimelberg HK (2006). Development of gap junctions in hippocampal astrocytes: evidence that whole cell electrophysiological phenotype is an intrinsic property of the individual cell. *J Neurophysiol* **96**: 1383–1392.

Schuchmann S, Schmitz D, Rivera C, Vanhatalo S, Salmen B, Mackie K *et al*. (2006). Experimental febrile seizures are precipitated by a hyperthermia-induced respiratory alkalosis. *Nat Med* **12**: 817–823.

Sim JA, Young MT, Sung HY, North RA, Surprenant A (2004). Reanalysis of $P2X_7$ receptor expression in rodent brain. *J Neurosci* **24**: 6307–6314.

Sperlágh B, Vizi ES, Wirkner K, Illes P (2006). $P2X_7$ receptors in the nervous system. *Prog Neurobiol* **78**: 327–346.

Stoop R, Surprenant A, North RA (1997). Different sensitivities to pH of ATP-induced currents at four cloned P2X receptors. *J Neurophysiol* **78**: 1837–1840.

Suadicani SO, Brosnan CF, Scemes E (2006). $P2X_7$ receptors mediate ATP release and amplification of astrocyte intercellular Ca^{2+} signaling. *J Neurosci* **26**: 1378–1385.

Surprenant A, North RA (2009). Signaling at purinergic P2X receptors. *Annu Rev Physiol* **71**: 333–359.

Tian GF, Azmi H, Takano T, Xu Q, Peng W, Lin J *et al*. (2005). An astrocytic basis of epilepsy. *Nat Med* **11**: 973–981.

Virginio C, Church D, North RA, Surprenant A (1997). Effects of divalent cations, protons and calmidazolium at the rat $P2X_7$ receptor. *Neuropharmacology* **36**: 1285–1294.

von Kügelgen I (2006). Pharmacological profiles of cloned mammalian P2Y-receptor subtypes. *Pharmacol Ther* **110**: 415–432.

Wang CM, Chang YY, Kuo JS, Sun SH (2002). Activation of $P2X_7$ receptors induced [^{3}H]GABA release from the RBA-2 type-2 astrocyte cell line through a Cl^-/HCO^{3-}dependent mechanism. *Glia* **37**: 8–18.

Wildman SS, King BF, Burnstock G (1998). Zn^{2+} modulation of ATP-responses at recombinant $P2X_2$ receptors and its dependence on extracellular pH. *Br J Pharmacol* **123**: 1214–1220.

Wirkner K, Günther A, Weber M, Guzman SJ, Krause T, Fuchs J *et al*. (2007). Modulation of NMDA receptor current in layer V pyramidal neurons of the rat prefrontal cortex by P2Y receptor activation. *Cereb Cortex* **17**: 621–631.

Wirkner K, Köfalvi A, Fischer W, Günther A, Franke H, Gröger-Arndt H *et al*. (2005). Supersensitivity of P2X receptors in cerebrocortical cell cultures after in vitro ischemia. *J Neurochem* **95**: 1421–1437.

Zhou M, Schools GP, Kimelberg HK (2006). Development of GLAST(+) astrocytes and NG2(+) glia in rat hippocampus CA1: mature astrocytes are electrophysiologically passive. *J Neurophysiol* **95**: 134–143.